Accepted Manuscript

Title: Production of high surface area mayenite (C12A7) via an assisted solution combustion synthesis (SCS) toward catalytic soot oxidation

Authors: Isaac Meza-Trujillo, François Devred, Eric M. Gaigneaux

PII: S0025-5408(19)30779-2
DOI: https://doi.org/10.1016/j.materresbull.2019.110542
Article Number: 110542

Reference: MRB 110542

To appear in: *MRB*

Received date: 6 May 2019
Revised date: 24 June 2019
Accepted date: 8 July 2019

Please cite this article as: Meza-Trujillo I, Devred F, Gaigneaux EM, Production of high surface area mayenite (C12A7) via an assisted solution combustion synthesis (SCS) toward catalytic soot oxidation, *Materials Research Bulletin* (2019), https://doi.org/10.1016/j.materresbull.2019.110542

Production of high surface area mayenite (C12A7) via an assisted solution combustion synthesis (SCS) toward catalytic soot oxidation

*Isaac Meza-Trujillo, François Devred and Eric M. Gaigneaux**

Institute of Condensed Matter and Nanosciences (IMCN), Université catholique de Louvain, Place Louis Pasteur, 1, box L4.01.09, 1348 Louvain-la-Neuve, Belgium

Graphical abstract

Graphical abstract

Synthesis of porous crystalline mayenite with high surface area and large pore volume at mild conditions with improved catalytic properties for soot oxidation

Highlights

- **Non-porous mayenite was directly obtained after combustion reaction using a fuels mixture**
- **Calcination temperature for mayenite formation was reduced from 1300 °C to 250 °C**
- **Porous mayenite was obtained from 275 °C by an assisted solution combustion method**
- **Mayenite crystallinity and texture were tuned by varying the calcination temperature**
- **Porous mayenite exhibited an enhanced catalytic performance in the soot oxidation**

Abstract

Mayenite ($Ca_{12}Al_{14}O_{33}$) is an attractive, non-expensive material, conventionally prepared over 1300 °C via solid-state reaction, producing a solid with low specific surface area (1 m^2/g).

Although a recent alternative allowed mayenite formation from 400 °C using hydrothermal method, it still requires a ball-milling step to increase the specific surface area (≥20 m^2/g), which is costly and energy-consuming, involving specialized equipment. Herein, we report a new, cost-effective and simple way to produce porous mayenite with enhanced textural properties at lower temperatures (~275 °C). Initially, non-porous mayenite was directly produced from 250 °C via a self-combustion reaction of nitrates with a double-fuel mixture. Furthermore, the addition of oxalic acid was implemented, obtaining porous mayenite after calcination of a preformed precursor and boosting its specific surface area and pore volume up to 74 m^2/g and 0.3 cm^3/g, respectively. Such textural enhancement notably increased mayenite catalytic properties in the soot oxidation reaction.

KEYWORDS: Solution combustion synthesis (SCS); porous mayenite; C12A7; X-ray diffraction; soot oxidation

1. Introduction

$12CaO{\cdot}7Al_2O_3$ ($Ca_{12}Al_{14}O_{33}$) is a calcium aluminate, labelled by the cement notation as C12A7, which was early identified as a constituent of the alumina cement.[1–4] In 1964, a mineral presenting an analogous chemical composition was discovered near Mayen (Germany) and so-called mayenite.[5] C12A7 crystal structure (cubic symmetry, space group I-43d, Z = 2, a = 11.989 Å, V = 1723.3 $Å^3$),[6] exhibits a peculiar three-dimensional framework tailored by AlO_4 tetrahedra partially interconnected by corner-sharing and some partially via Ca bridges, where Ca^{2+} is octahedrally coordinated.[7] C12A7 unit cell displays a positively charged

framework, conventionally, denoted as $[Ca_{24}Al_{28}O_{64}]^{4+}$, composed by 12 interconnected cages (i.d. ~0.4 nm); the formal charge per cage is +1/3. In stoichiometric conditions, two extra-framework "free" oxygen anions (O^{2-}) are clathrated and statistically distributed, one per six cages, to compensate the positive charge.[8–10] These “free” oxygen anions are loosely bound by electrostatic interactions and coordinated by six Ca cations inside the cages.[7] Hence, they can be easily replaced by more reactive oxygen species such as O^-,[11–15] O_2^-,[10–13,15] and O_2^{2-},[16,17] or by monovalent anions such as OH^-,[18] H^-,[19] F^-,[8] Cl^-,[8,20] S^{2-},[20] CN^-,[20] and even electrons giving an electride.[21] These partial or “total” exchanges can be done by controlling synthesis conditions in terms of atmosphere composition and annealing temperature.[13]

Over the last decades, mayenite has attracted the attention, regarding its unique features such as high ionic conductivity,[9,22] anion exchangeability,[8,10,20] and oxidative catalytic properties[23–28] attributed to the presence of the above mentioned "free" oxygen species. Moreover, C12A7 has exhibited high resistance to carbon deposition and anti-sulphur poisoning properties ascribed to the existence of clathrated O_2^- and O_2^{2-} species which are formed by the interaction of the “free” oxygen species with atmospheric oxygen at temperatures over 400 °C.[13,15,24,29]

Mayenite was first synthesized, by the ceramic route, via a solid-state reaction between $CaCO_3$ and γ-Al_2O_3 at 1350 °C.[1] Since then, the ceramic route has been widely used as a classical pathway to obtain C12A7. Nevertheless, this method unavoidably implies very high temperatures over 1300 °C and long calcination times ranging from several hours to days, with intermediate crushing steps compulsory if a single phase is desired.[1,9,10,30] Because of such synthesis protocol, C12A7 obtained so far shows a negligible porosity and a very low specific surface area,

rarely exceeding 1 $m^2 g^{-1}$, leading to poor catalytic performances (e.g. low conversion), and limit its use as a potential support for other catalytic species.[31]

Recently, much research has been seeking for new synthesis approaches to produce porous C12A7 powder at milder conditions, especially at lower temperatures. Sol-gel strategies including a modified-Pechini method,[32] citrate route,[33] and oxalate precursor[34] have been attempted. For instance, extended periods of ball-milling has been added to improve the specific surface area of the powders derived from sol-gel or ceramic routes.[24,35] A recent alternative via a hydrothermal method was reported as a low-temperature technique to produce porous mayenite.[36] However, this method still requires a planetary ball-milling procedure to homogenize the aqueous suspension of hydroxides and to increase the specific surface area of the final product. This kind of milling is a costly, energy-consuming process that involves specialized equipment, which could limit the scalability of this synthesis method.

Besides these approaches, the solution combustion synthesis (SCS) appears as a suitable and attractive method because it is a cheap, fast, energy effective and easily scalable process.[37–43] Various authors already used the combustion method to prepare mayenite via a single fuel approach by mixing Al and Ca nitrates with urea or glycine.[14,39–41,43] Yet, the direct production of mayenite after the combustion reaction was never possible without a post-annealing treatment which, again, requires high temperatures.

In this context, our research aims and succeeds at producing pure crystalline mayenite directly after the SCS without any additional post-thermal treatment required, thanks to a novel double-fuel mixture method. Moreover, a modification in the previous method by the addition of oxalic acid makes possible the production of mesoporous C12A7 with a unique specific surface area

compared to the ceramic route, all this without requiring long annealing times at high temperatures nor costly, energy-consuming milling (or any other) processes. Moreover, the benefit of our synthesis method on the mayenite catalytic properties is demonstrated in the framework of an oxidation reaction using carbon black as a surrogate molecule to simulate the soot oxidation. Particulate matter (PM) emissions from diesel engines is a relevant topic to the strike against anthropogenic pollution. PM is mainly composed of soot particles and it can cause serious environmental and health problems.[44] In general, diesel soot particles are removed by a post-treatment process which combines the use of a particulate filter and an oxidation catalyst usually composed by supported noble metal NPs and/or rare metal oxides. [45,46] The catalytic soot oxidation is a complex process that occurs at the interface contact boundary of three counterparts (catalyst, soot and gas mixture). Consequently, the catalytic activity in the soot oxidation is highly affected by two main features: the contact quality between the soot particles and the catalyst and the adequate transfer of the so-called active oxygen species from the catalyst surface to the soot particle to further oxidize it into less harmful molecules such as CO_2 . [47–50] Thus, the texture and structure of catalysts at a nanoscopic level play an important role in deep oxidation reactions. In this scenario, the development of cost-effective catalysts not noble/rare metal based with improved texture and controlled morphology are highly desired.

2. Materials and Methods

2.1. Materials

Calcium nitrate tetrahydrate ($Ca(NO_3)_2 \cdot 4H_2O$, 99.9%), aluminum nitrate nonahydrate ($Al(NO_3)_3 \cdot 9H_2O$, 98.5%), urea (CH_4N_2O, 99.9%) and β-alanine ($C_3H_7NO_2$, 99%), were purchased from Merck. Anhydrous oxalic acid ($C_2H_2O_4$, 99.9%) was purchased from Sigma Aldrich. All products were used as delivered without any further treatments.

2.2. Mayenite via the solution combustion synthesis (SCS-C12A7)

Mayenite powders synthesized by the SCS technique is outlined below. In this study, hydrate nitrates were chosen as sources of Ca and Al since they contain the oxidizing agent (NO_3^-), which is fundamental for the redox reaction, but also because they are highly soluble in water allowing the formation of a homogenous solution. Besides, urea and β-alanine were selected as suitable fuels for the combustion reaction with aluminum and calcium nitrates, respectively. Ianoş et al. reported that calcium nitrate and aluminum nitrate exhibit a different reactivity with respect to urea and β-alanine, allowing the direct formation of C3A after the combustion reaction, compared to the use of a single-fuel.[51]

According to both the propellants chemistry and related thermodynamics calculations CO_2, N_2 and H_2O are assumed to be the most stable gaseous products over other plausible compounds.[52–54] In a first glance, two combustion reactions can be obtained assuming that both nitrates react in separate way with each fuel.

$$12\ Ca(NO_3)_2{\cdot}4H_2O + 14\ Al(NO_3)_3{\cdot}9H_2O + n\ CH_4N_2 + (3/2\,n - 165/2)\ O_2 \rightarrow Ca_{12}Al_{14}O_{33} + n\ CO_2 + (174+2n)\ H_2O + (33+n)\ N_2 \quad (1)$$

$$12\ Ca(NO_3)_2{\cdot}4H_2O + 14\ Al(NO_3)_3{\cdot}9H_2O + m\ C_3H_7NO_2 + (15/4\,m - 165/2)\ O_2 \rightarrow Ca_{12}Al_{14}O_{33} + m\ CO_2 + (187 + 7/2\,m)\ H_2O + (33 + m/2)\ N_2 \quad (2)$$

Then, following the method proposed by Jain regarding the propellant chemistry, it is possible to calculate the elemental stoichiometric coefficient (Φ).[52] The latter, also referred as fuel-to-oxidizer ratio, is the ratio between the total oxidizing and reducing valencies of the oxidizers (nitrates) and reducers (fuels). In this redox mixture, the fuel/oxidizer ratio controls the

consumption or production of oxygen during the combustion. Under stoichiometric conditions, no molecular oxygen is required (Φ = 1). While, Φ > 1 a supply of molecular oxygen is needed, meaning fuel-rich conditions. Besides, when Φ < 1 molecular oxygen is produced, denoting fuel-lean conditions. Therefore, assuming stoichiometric conditions the required moles of fuels n and m can be expressed in terms of the fuel-to-oxidizer ratio, thus for Eq. (1) Φ = n/55 whereas for Eq. (2) Φ = m/22. The overall combustion is given by the addition of Eqs. (1) and (2), as follows:

$$12\ Ca(NO_3)_2 + 14\ Al(NO_3)_3 + 55/2\ \Phi\ CH_4N_2O + 11\ \Phi\ C_3H_7NO_2 + 165/2\ (\Phi-1)\ O_2 \rightarrow$$
$$Ca_{12}Al_{14}O_{33} + 121/2\ \Phi\ CO_2 + 187/2\ \Phi\ H_2O + 33\ (\Phi+1)\ N_2 \qquad (3)$$

In a typical synthesis, all the reagents were calculated to produce 5 g of mayenite. Therefore, stoichiometric amounts of metal nitrates (Ca/Al:12/14) were dosed in a borosil vessel (500 mL), followed by the addition of varying amounts of urea and β-alanine, corresponding to different Φ ratios between 0.5 and 1.5, but always keeping a constant molar ratio between the fuels (urea/β-alanine:5/2). Then, 10 mL of distilled water was poured, and the redox mixture was stirred and heated up to 50 °C on a hot plate until a clear solution was obtained. Subsequently, the vessel was introduced into a pre-heated furnace and kept at constant temperature in the range of 250-500 °C, where the solution underwent dehydration. By the time, the solution started to boil and swell, releasing large amounts of fumes, and leading to a frothing gel. Once, the ignition temperature was attained, an exothermic self-sustaining reaction took place, giving way to the desired product. The whole process was completed after 1.5-25 min, depending on the furnace temperature. However, the time between the actual ignition and the end of the combustion reaction always just took a few seconds (~15 s). The operation conditions had an impact not only over the

intensity of the reaction, but also over the morphology and density of the product, depending on the selected fuel-to-oxidizer ratio. For example, under stoichiometric condition (Φ = 1), the obtained product was a dense colorless coral-like solid, whilst at lean or fuel-rich conditions the products were voluminous colorless or greyish powders, respectively. Finally, the as-burnt powder was quenched to room temperature, grinded in agate mortar, sieved and stored for further characterization.

2.3. Porous mayenite via an assisted solution combustion synthesis (@SCS-C12A7)

In a second stage, oxalic acid was introduced into the synthesis aiming an enhancement in the textural properties. The above-calculated stoichiometric precursor amounts (Φ = 1) were added in a borosil vessel. Additionally, a varying amount of oxalic acid ($C_2H_2O_4$, afterward noted as OA) was added, which is reported as a mass ratio between the amount of OA and the calculated amount of C12A7, ranging from 0.25-1. All reagents were dissolved in hot distilled water and kept at 80 °C under magnetic stirring on a hot plate to obtain a homogeneous solution. Then, the solution was placed in a pre-heated furnace at 500 °C where the combustion reaction occurred. The SCS-derived powder was quenched to room temperature, then it was hydrated for about 20 min with hot distilled water (80 °C), filtered and dried at 110 °C overnight. Finally, the as-dried solid was crushed and calcined in a pre-heated furnace in the range of 300-800 °C for 4 hours under static air.

2.4. Characterizations

Powder X-ray diffraction (XRD) analysis was performed on a Bruker-D8 advance diffractometer with a Bragg-Brentano geometry, using a LynxEye XE-T detector with Cu Kα radiation

(λ=0.15418 nm, 40 kV, 30 mA). The samples were scanned in a 2θ range between 5° and 80° at a scanning rate of 2.2°/min. A XRD study measured at various temperatures was carried out using an XRK 900 (Anton Paar) chamber module with a heating rate of 10 °C min^{-1}, from room temperature (25 °C) to 800 °C under synthetic dry air flow (alphagaz1: 80% N_2 , 20% O_2 , Airliquide). The phases identification was done using the PDF2-2004 database, while the crystallography data for the Rietveld analysis were taken from the Crystallography Open Database (COD).[55] The crystallite size was calculated from (211) the strongest reflection (2θ = 18.11°), using the Scherrer equation, $L = 0.9 \lambda / \beta \cos \theta$, where L is the crystallite size in Å, β is the full-width at half-maximum (FWHM) of the Bragg peak (211) plane corrected for instrumental broadening in radians, λ is the wavelength of Cu Kα and θ is the Bragg angle.

Rietveld quality powder X-ray diffraction patterns were obtained in a 2θ range: 10-100° at a scanning rate of 0.0075°/min. A pseudo-Voigt function for the modelling of the peak profile was used during the refinement, while the background was manually selected and not refined. The Rietveld analysis was performed i) to determine the weight fractions of each observed phase in the SCS-derived powders and ii) to calculate the lattice parameters of C12A7. The FullProf suite and its graphical tool Winplotr were used to accomplish the refinements.[56,57]

The textural properties were evaluated by molecular nitrogen physisorption using a Micromeritics Tristar 3000. Prior the analysis, roughly 0.15 g of sample were degassed overnight under vacuum (6.6 Pa) at 150 °C. The measurements were performed at -196 °C in the relative pressure range of 0.01-0.99 (p/p_0). The specific surface area (SSA) was calculated from the adsorption isotherm branch using the Brunauer-Emmet-Teller (BET) method. The pore size distribution, average pore diameter and pore volume were calculated by the Barrett–Joyner–Halenda method (BJH) using the data from the desorption isotherm branch.

Scanning electron images were recorded on a JEOL 7600F microscope working between 10-15 kV to analyze the morphology of the samples. Prior to the analysis, the powdered samples were placed on a piece of carbon black tape on an aluminum stub. A chromium sputter coating of 16 nm was carried out under vacuum with a Sputter Metal 208HR (Cressington).

2.5.Catalytic activity assessment

The catalytic activity of C12A7 samples for soot oxidation was performed in a Hiden Analytical Catlab microreactor module coupled with a Hiden Analytical QGA mass spectrometer. The temperature-programmed combustion (TPC) was evaluated at atmospheric pressure between 50-800 °C with a heating rate of 10 °C min^{-1}. The gas mixture flow (50 mL min^{-1}) was composed of 5% O_2 diluted in He (Praxair). A commercial carbon black (CB) powder (Printex U, Degussa), which has been widely used as diesel soot model, was selected in this study.[45,46,58] A total mass of 50 mg was prepared by mixing 5wt% of CB with powdered catalyst (<56 μm). A tight contact procedure was accomplished by mixing the powders in a mortar for 10 min, in a way to guarantee good reproducibility during the tests and to allow consistent comparisons between the catalysts. Then, the mixture was placed inside a quartz tube microreactor (i.d. ~ 0.4 mm) between two layers of silica wool. The temperatures corresponding to the start of the oxidation process (T_{onset}) and to the CO_2 maximal concentration peak (T_p) were taken as an index of the catalytic activity for each tested catalyst. The lower the T_p value, the more active the catalyst. Besides, the selectivity of the different catalysts was obtained by relating the produced amounts of CO_2 and CO to the total conversion of soot. The total amount of each product was calculated by integrating the area under the curves of CO_2 and CO from TPC runs. Thus, the selectivity was calculated using the following equation.

$$S_{CO_x} = CO_x / (CO + CO_2) \times 100(\%) \quad (7)$$

3. Results and discussion

3.1. Mayenite production via the SCS method

At first glance, the combustion reaction between Ca and Al nitrates with the fuel-mixture of urea and β-alanine, under stoichiometric condition (Φ = 1), leads to the direct formation of C12A7 from 250 °C as revealed by the XRD patterns (Figure 1), which displays C12A7 (JCPDS-card 09-0413) as the major phase. The calculated lattice parameter (a) for all the samples varies between 11.974-11.977 Å (Table 1), which proves to be slightly smaller than the value reported in the literature for pure synthetic mayenite (a=11.989 Å)[6–8], implying the presence of C12A7 phase. Nevertheless, to obtain a C12A7 single phase, an appropriate furnace temperature to trigger the combustion reaction should be selected. As shown in the zoom inset (Figure 1), an increase in the furnace temperature from 250°C to 500°C promotes the disappearance of the side phases, namely monocalcium aluminate ($CaAl_2O_4$: CA) and tricalcium aluminate ($Ca_3Al_2O_6$: C3A). This observation is supported by the reduction of the intensities of the strongest reflection peaks of CA (JCPDS-card 23-1036) and C3A (JCPDS-card 38-1429) at 30.09° (123) and 33.20° (440), respectively.

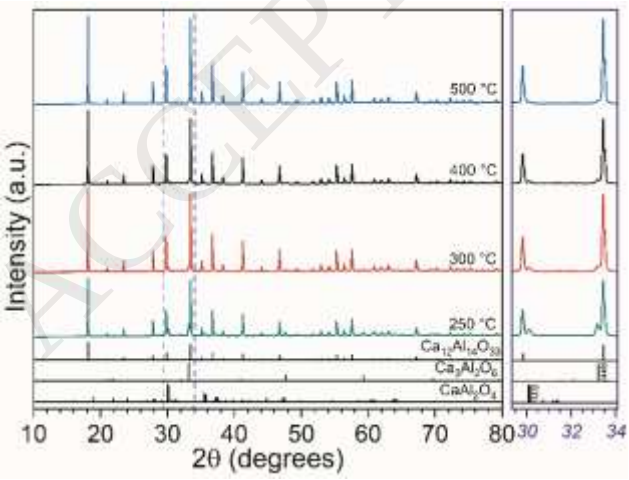

Figure 1. XRD diffractograms of the as-synthesized powders from the SCS at different temperatures. Inset zoom in the 2θ range between 28-34°

A quantification of the three crystalline phases C3A, CA and C12A7 was accomplished by Rietveld refinement and summarized in Table 1. The results second the above stated showing an increase in the C12A7 content with the rise of the furnace temperature, producing in matter of minutes (1.5 min) a well-crystalline highly pure C12A7 (98%) at 500 °C. Moreover, the well-developed crystallinity of the SCS-derived C12A7 is visually validated by the sharpness of the XRD peaks (Figure 1) and, settled by the reported values for the crystallite size (Table 1.), calculated from the (211) strongest peak (2θ=18.11°) using the Scherrer equation, which ranges between 110-122 nm. All these results reinforced the fact that the direct formation of C12A7 is possible due to the high temperature reached during the combustion reaction involving urea and β-alanine as fuels, making that no additional post-thermal treatments are required.

At lower temperatures as 250 °C, the duration of the whole process until the combustion reaction occurs, is prolonged (Table 1), mostly due to a lower evaporation rate of the solvent, which probably favors a slight depletion of the most thermo-sensible reagents. According to the literature, urea thermally decomposes between 134-263 °C yielding ammonia (NH_3) and isocyanic acid (HCNO) as principal products.[59] In addition, $Al(NO_3)_3 \cdot 9H_2O$ melts at 80 °C and starts to decompose from ~100-150 °C.[60] Hence, the urea and aluminum nitrate partial decomposition could provoke their premature depletion, considering the longer duration (25 min) of the entire process. As consequence, at temperatures below 500 °C the calculated fuel-to-oxidizer ratio ($\Phi = 1$) could be unbalanced by the occurrence of these side depletions, prompting the formation of CA and C3A. Besides, regarding the $CaO\text{-}Al_2O_3$ phase diagram,[1–4] the operating region to attain a C12A7 single phase is quite narrow and highly dependent on the temperature and

stoichiometric ratio of CaO: Al_2 O_3 . So, the heat losses at lower temperatures could have also overcome the amount of energy released by the exothermic reaction, lowering the attained temperature during the combustion process.

Table 1. SCS parameters, crystallite size, lattice parameter and phase quantification of the SCS derived C12A7 powders produced at different temperatures with Φ = 1

Sample	Temperature (°C)	Total process time (min)	Crystallite size (nm)	a (Å)	C12A7 (%)	C3A (%)	CA (%)
SCS-C12A7-25	250	25	110	11.974	79	10	11
SCS-C12A7-30	300	10	116	11.977	92	3	4
SCS-C12A7-40	400	4	117	11.974	94	3	3
SCS-C12A7-50	500	1.5	122	11.975	98	1	1

The measured SSA for all the C12A7 derived from the SCS between 250-500°C, were equal or even less than 1 m^2 g^{-1}. These reported surface areas are characteristics of non-porous materials, which are alike with those previously stated for mayenite synthesized via the ceramic route.[31] According to the literature, SCS method usually allows the formation of nanoporous powders as combining two main factors: i) the generation of large amounts of gases during the combustion reaction, and ii) the fast cooling rate once the combustion temperature is attained.[38] As consequence to these features, a significant volumetric expansion in the solid product usually takes

place, preferring the formation of finely dispersed nanoparticles, while preventing their agglomeration. Despite these issues, the SCS of C12A7 under stoichiometric conditions (Φ = 1) using urea and β-alanine, does not lead to producing a porous material probably due to high temperature attained during the combustion reaction, which promotes the sintering of the grains.

The morphology and microstructure of the SCS-derived C12A7 powders were investigated by scanning electron microscope (SEM) and are illustrated in the Appendix A (see Figure. A.1). The SCS-C12A7-50 sample presents a heterogeneous mixture of irregular shaped aggregates conformed by partially sintered grains and dense solid particles within a large size distribution (1-100 μm). At higher magnifications, the presence of small superficial pores and craters was observed, which were probably left behind after the sudden evaporation of trapped droplets coming from aqueous solution during the combustion reaction. In the samples synthesized at temperatures below 500°C similar morphologies and microstructures were recognized. SEM observations confirm that after the combustion reaction the yielded product is composed of sintered dense particles, which drastically reduces the specific surface area.

The XRD patterns (Figure 2) indicate that the direct production of C12A7 was possible when Φ ranges between 0.75 to 1.25, whereas variations out of this range favored the formation of an amorphous powder. Besides, the Rietveld analysis of the crystalline samples (Φ = 0.75 and 1.25) revealed that the mayenite content slightly decreases by this modification (see Table A.1, Appendix A). The modification of the fuel-to-oxidizer ratio was accomplished to increase the specific surface area by preventing the sintering of the preformed grains after combustion, as reported in literature during the production of porous solids via the SCS under rich-fuel conditions.[53,61] However, no improvement in the specific surface area was observed, displaying

similar values to those above reported in the solution combustion of C12A7 with a fuel-to-oxidizer equal to 1.

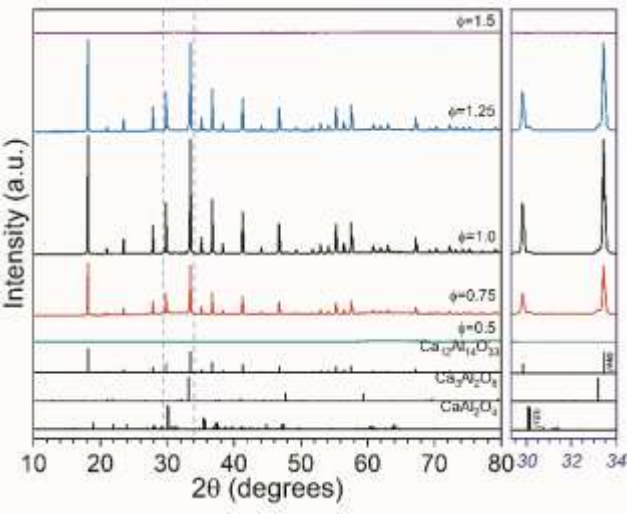

Figure 2. XRD diffractograms of the as-synthesized powders from the SCS at 500°C with different fuel/oxidizer ratios. Inset zoom in the 2θ range between 28-34°

3.2. Porous mayenite production via an assisted solution combustion method

A new approach to produce porous mayenite via a modification in our former SCS protocol was accomplished, by adding oxalic acid (OA). A previous study, related to the synthesis of cobalt ferrite ($CoFe_2O_4$), suggests that oxalic acid can act as porogeneous and combustion retarding agent, leading to an improvement of the textural properties.[62] The combustion mode and the morphology of the as-obtained powder (Figure 3), vary with the increasing amount of OA. At low concentrations (0.25 g OA/g C12A7), the combustion reaction takes place as a thermal explosion (Figure 3a), where an incandescent intense flame is observed. While, at higher OA concentrations (≥0.5 g OA/g C12A7), the reaction proceeds via a self-propagating smoldering combustion (Figure 3b and c), where a small portion of the frothing gel locally started the reaction and propagated it in a wave through the rest of the volume.[38] The morphology of the as-obtained powders varies

from a dense colorless coral-like solid (Figure 3d) passing for a fluffy volatile whitish powder (Figure 3e) through a highly voluminous blackish powder (Figure 3f). The latter overflowed the container, while its coloration denoted the presence of residual carbon due to the excess of fuel.

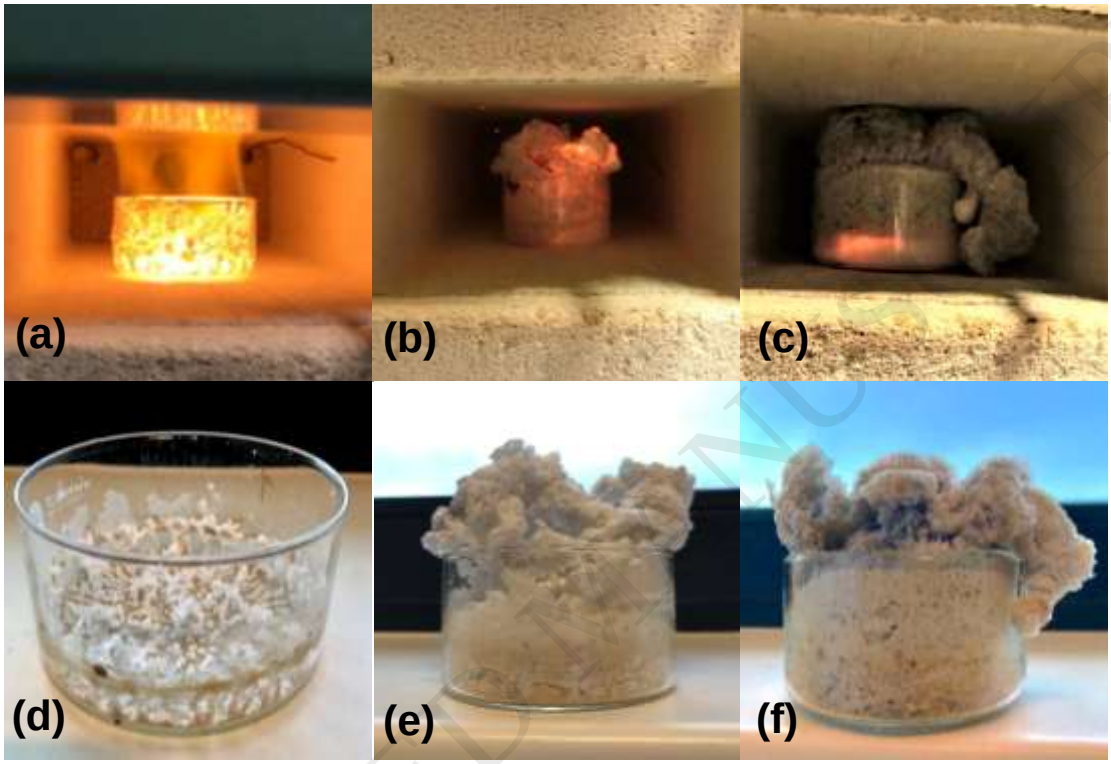

Figure 3. Images from the combustion reaction with different OA ratios of a) 0.25, b) 0.5 and b) 0.75 g OA/g C12A7. Images of the as-burnt products with different OA ratios c) 0.25, d) 0.5 and e) 0.75

XRD patterns (Figure 4) show that the direct formation of C12A7 after the assisted SCS with addition of OA was only possible when 0.25 g OA/g C12A7 were added, displaying a well-crystallized C12A7 with the minor presence of CA and C3A. These results are consistent with those above discussed when fuel-rich conditions were used ($\Phi > 1$). Besides, OA ratios higher than 0.25 denote the formation of an amorphous powder. The morphology of the powders and the loss

of crystallinity can be explained by i) the substantial upsurge of the gas volume evolved during the combustion reaction, and ii) by a marked reduction in the combustion temperature. Even when oxalic acid was added, a ratio of 0.25 g OA/g C12A7 does not lead to any improvement in the textural properties. However, at higher OA concentrations, the BET surface area of the SCS-derived amorphous powders was improved, displaying values in the rage of 9-12 $m^2\ g^{-1}$. The amorphous voluminous powder obtained after the SCS with 0.5 g OA/g C12A7 was selected for the following as no significant improvement was further attained with higher OA concentrations.

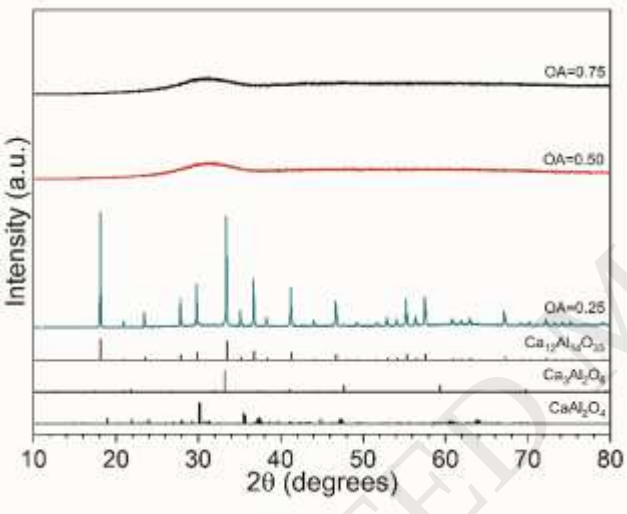

Figure 4. XRD diffractograms of the as-synthesized powders from the assisted SCS with different OA ratios

The @SCS-derived amorphous powder was then hydrated, filtered and dried. The XRD pattern (Figure 5) of the as-dried preformed precursor (@SCS-P-RT) obtained at room temperature (RT), shows the presence of three crystalline phases: tricalcium aluminate hexahydrate (hydrogarnet) $Ca_3\ Al_2\ (OH)_{1\ 2}$ (JCPDS-card 24-0217), aluminum hydroxide (gibbsite) $Al(OH)_3$ (JCPDS-card 33-0018) and calcium carbo aluminate hydrate (carbo-aluminate) $Ca_4\ Al_2\ (OH)_{1\ 2}\ CO_3 \cdot 5H_2\ O$ (JCPDS-card 41-0219).

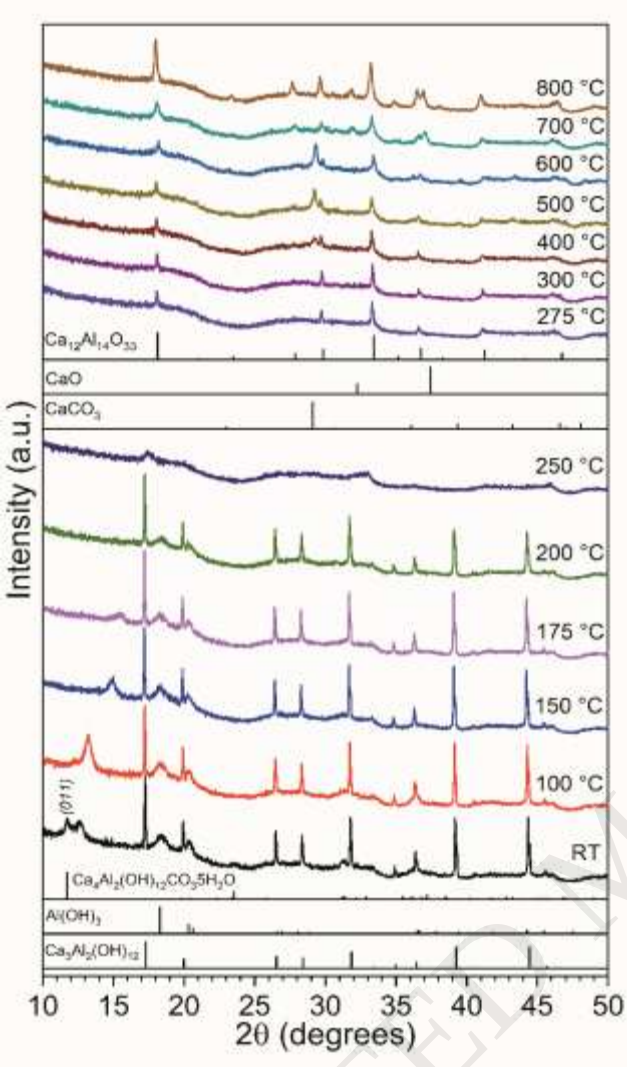

Figure 5. XRD patterns collected at different temperatures for the as-dried preformed precursor from room temperature (RT) to 800 °C

In previous studies, during the production of mayenite via a hydrothermal method, the formation of $Ca_3Al_2(OH)_{12}$ with an excess of $Al(OH)_3$ has been also reported after a hydrothermal treatment of a mixture of calcium and aluminum hydroxides.[23,36] Li et al. suggested that the presence of $Ca_3Al_2(OH)_{12}$ could favor the formation of C12A7 at lower temperatures.[36] Besides, we hypothesized that the formation of $Ca_4Al_2(OH)_{12}CO_3 \cdot 5H_2O$ could take place during the hydration of the powder due to the presence of an amorphous carbonate phase left after

combustion reaction. Furthermore, the XRD pattern of @SCS-P-RT shows an unidentified peak partially superposed to the strongest reflection (011) of the carbo-aluminate phase. This could be attributed to a partial dehydration of $Ca_4Al_2(OH)_{12}CO_3 \cdot 5H_2O$ during the drying step.

The calcination process of @SCS-P-RT was followed by a X-ray diffraction study carried out at different temperatures as illustrated in Figure 5. XRD patterns between 100-200 °C show that the main reflection of carbo-aluminate, as well as the partially superposed peak observed at room temperature, were vanished. In contrast, a new peak at higher angle was formed, which shifts even towards higher angle with the rise of the temperature, until its disappearance at 200 °C. In previous studies, carbo-aluminate has been described as a lamellar structure characterized by the presence of stacked positively charged brucite-like layers of $[Ca_4Al_2(OH)_{12}]^{2+}$ and negatively charged interlayers of $[CO_3 \cdot 5H_2O]^{2-}$. It has also been stated that its basal spacing thickness depends on the shape and size of the anions and the amount of interlayer water. Hence, it seems that the loss of the interlayer trapped water molecules during the heating step reduces the basal spacing thickness (7.55 Å), shifting the corresponding reflection towards higher angles.[63,64] Thus, these previous finding could explain our observations. In contrast, the hydrogarnet phase remains stable up to 200 °C, while the gibbsite peaks seem less intense with the rise of temperature probably due to loss of structural water. It has been suggested that $Al(OH)_3$ dehydrates from ~300 °C forming AlO(OH) (boehmite); however, its presence is not noticed in our study.[36] At 250 °C, an almost amorphous powder is observed with the presence of a poorly-crystalline hydrogarnet. A slight increase in the temperature to 275 °C then leads to the formation of mayenite phase. Furthermore, the emergence of calcium carbonate (calcite) $CaCO_3$ (JCPDS-card 05-0586) as an impurity is evidenced from 400 °C up to 600 °C, whilst a further increase in the calcination temperature promotes the formation of calcium oxide (lime) CaO (JCPDS-card 37-1497) via the decarbonation

reaction of calcite. Finally, it was noticed that mayenite crystallinity is favored by the rise of temperature seconding the formation of a well crystallized mayenite at 800 °C displaying an average crystallite size of 33 nm according to Scherrer's equation. A further Rietveld analysis (see Figure A.2 in the Appendix A) showed that the powder obtained at 800°C is mainly composed of mayenite with a content of 93% with the presence of CaO as a concomitant phase (see Table A.2 in the Appendix A).

From the above XRD study four calcination temperatures were selected for further characterization by N_2 physisorption. The materials were thus characterized after being calcined for 4 h under static air. The N_2 physisorption results for the as-dried preformed precursor and the calcined samples show isotherms of type IV (Figure. A.3), which are characteristics of mesoporous materials according to the IUPAC classification. Additionally, all the reported adsorption-desorption isotherms display hysteresis loops of type H3, which correspond to materials composed of non-rigid aggregates with internal porosity within slit-shaped pores.

The detailed textural properties of the calcined samples are summarized in Table 2. The as-dried preformed precursor (@SCS-P-RT) shows a higher BET surface area (33 $m^2 g^{-1}$) compared to the fluffy @SCS-derived amorphous powder obtained directly after the combustion reaction (9 $m^2 g^{-1}$). This enhancement in the specific surface area could be attributed to the rearrangement of the atoms during the formation of three crystalline phases after the hydration and drying processes. Thus, the calcination of @SCS-P-RT at lower temperatures as 300 °C allows the formation of mesoporous mayenite presenting a notably high pore volume of 0.22 $cm^3 g^{-1}$, which became enlarged as the temperature increases up to 600 °C, whereas calcination beyond this temperature slightly decreased the cumulative pore volume. Moreover, the BET surface area increases with calcination temperature up to 400 °C, where a remarkable value of 74 $m^2 g^{-1}$ is

displayed. However, at higher temperatures the BET surface area decreases, while the mayenite crystallinity is favored as shown before by the XRD study at different temperatures. Thus, at 800 °C a highly pure crystalline mesoporous C12A7 is obtained revealing a specific surface area 30-fold higher than those obtained through the conventional ceramic route.

Table 2. Textural properties of the as-dried preformed precursor and of the calcined mayenite samples at different temperatures for 4 h

Sample	Calcination temperature (°C)	SSA ($m^2\ g^{-1}$)	BJH cumulative pore volume ($cm^3\ g^{-1}$)	Average pore diameter (nm)
@SCS-P-RT	-	33	0.23	24
@SCS-C12A7-30	300	55	0.22	29
@SCS-C12A7-40	400	74	0.29	24
@SCS-C12A7-60	600	52	0.31	22
@SCS-C12A7-80	800	30	0.26	33

By contrast, the pore size distribution was enlarged with the rise of the temperature. This could be explained by a shrinking of intragranular spaces during the calcination considering non-rigid structure that these samples present. Nevertheless, at 600 °C the sample presents a narrower pore diameter of ~22 nm, this issue is likely related with the decarbonation reaction which takes place at that temperature by transforming $CaCO_3$ into CaO with the release of CO_2 , leading to the formation of narrowed pores.

The SEM images (Figure 6a) of the calcined sample at 800 °C second the N_2 physisorption results showing the presence of non-rigid agglomerates of flake-shaped nanoparticles. At higher magnification (Figure 6b), it was possible to observe that the flake-shaped particles are smaller than 100 nm. A similar structure was observed during the production of mayenite by a sol-gel oxalate precursor method.[34] Thus, probably the use of oxalic acid during the preparation of mayenite leads to the formation of this particular kind of structure.

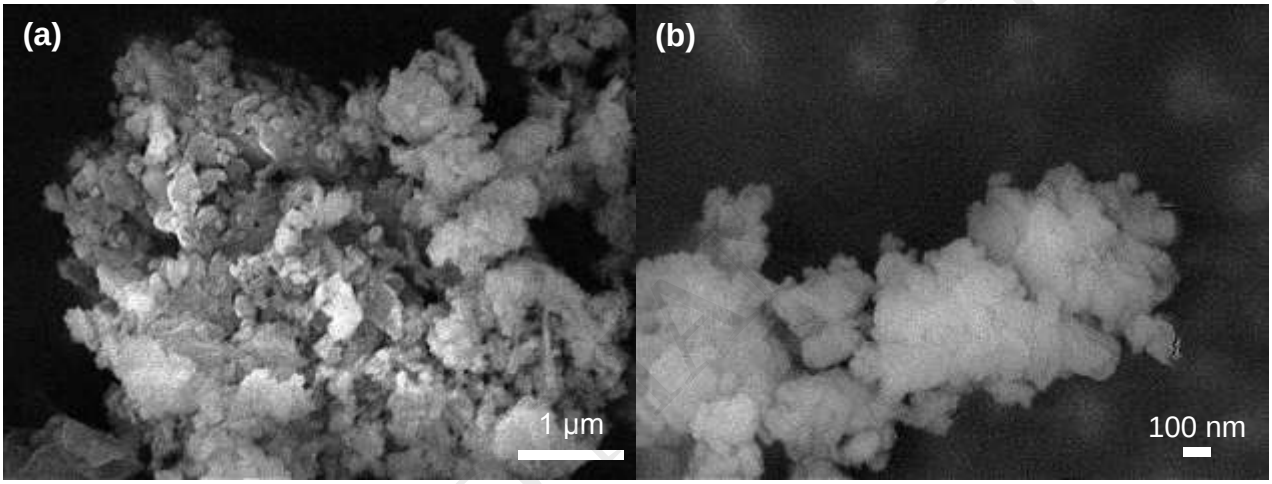

Figure 6. Scanning electron microscope (SEM) images of mayenite calcined under static air at 800 °C for 4 h with different magnifications a) 20000x and b) 55000x

3.3. Evaluating the catalytic activity of mayenite in the soot combustion

The catalytic activity of C12A7 was evaluated during the combustion of soot, to enlighten any improvement in the performances related to the enhancement of its specific surface area. In this study, a tight contact between the soot and C12A7 particles was used because it ensures in our opinion a better reproducibility than loose contact conditions when preparing the solid mixture (catalyst with soot), even though it is a less representative approximation of the contact between soot particles and catalyst in realistic conditions. Besides, tight contact allows a better

understanding of the intrinsic reactivity which are imperative to draw reliable comparisons between the different catalysts, as reported in the literature. [45,58]. Table 3 gathers the results of the performed soot oxidation TPC runs with different C12A7 catalysts, along with an uncatalyzed run (α-alumina) as reference: the onset and peak temperatures, as well as the selectivities towards CO_2 and CO during the soot oxidation are here summarized. During this catalytic study, porous mayenite sample (@SCS-C12A7-40) was not employed considering that it still presents a considerable amount of calcium carbonate as depicted by the XRD study (Figure 5). Thus, the quantification of the total CO_2 amount produced by the soot oxidation would not be accurate enough. An additional argument is that the texture of the material will change during the catalytic test due to the exposition of the sample at temperatures over its calcination temperature, modifying in this way the specific surface area of the sample, and therefore making the interpretation of the performance of this peculiar sample unambiguous. Additionally, to illustrate the performance of the different C12A7 catalysts the TPC curves of CO_2 and CO (inset) produced during the soot combustion are plotted in Figure 7.

In the absence of a catalyst, Printex-U combustion began around 486 °C followed by a gradual increase in the production of CO_2 with further increments in the temperature, reaching a maximum at 655 °C. In the presence of non-porous mayenite (SCS-C12A7-50, 1 $m^2\ g^{-1}$) the combustion process is shifted to lower temperatures showing a catalyzed total oxidation at 571 °C. Furthermore, as expected, a remarkable improvement in the activity was then observed, when porous mayenite was employed. In this scenario, a reduction on the T_{onset} of 81 and 49 °C with respect to the non-catalytic combustion, was recorded for the mayenite samples calcined at 600 and 800 °C, respectively. Likewise, a more noteworthy reduction on the peak (T_p) was evidenced, dropping from 600 °C to 488 and 514 °C, respectively. These decreases, in the T_{onset} and T_p values,

evidence that an enhancement of mayenite texture, as well as the presence of nanoscopic particles, positively favors the catalytic performance of mayenite during the soot total oxidation. Our statements are supported by a previous study in which Yang et al. suggested that the desorption of reactive oxygen species in mayenite occurs more readily with decreasing the particle size. Indeed, they found that the mobility and further desorption of oxygen species is limited by mass transport in the bulk. Therefore, the presence of smaller particles shifted the oxygen desorption to lower temperatures promoting in this way the diffusion of the oxygen species towards the surface.[13]

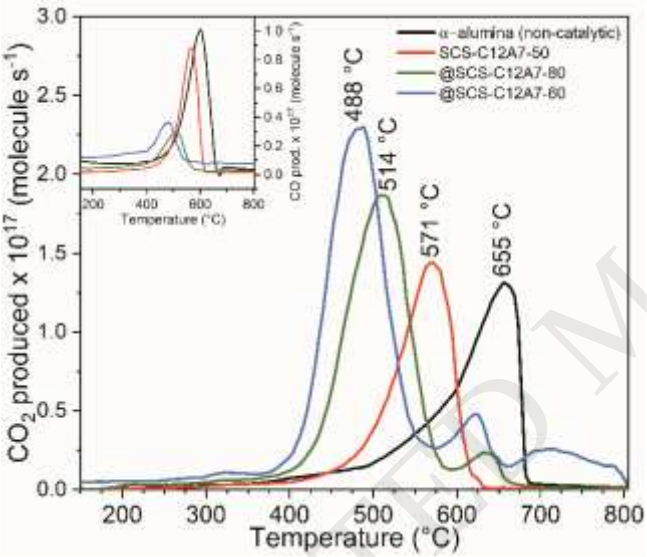

Figure 7. CO_2 and CO (inset) produced during the catalytic oxidation of soot (Printex- U); porous mayenite calcined at different temperatures 600 °C (blue) and 800 °C (green); as-synthesized non-porous mayenite obtained after the combustion reaction at 500 °C (red); non-catalytic soot combustion is also displayed for comparison (black)

Moreover, as mentioned in the introduction, these "free" oxygen species interact with atmospheric oxygen at the interface of the outermost layer of mayenite to form reactive oxygen species (O_2^-, O_2^- and O_2^{2-}) at temperatures over 400°C.[11,15] Thus, supported on these facts and

considering that the catalytic soot oxidation took place at temperatures in the same range at which the reactive oxygen species are formed, it is consistent to consider these oxygen species as the active sites for the soot oxidation over mayenite. On the other hand, the small peaks in the region of 580-800 °C could be explained by the release of CO_2 due to the decarbonation of $CaCO_3$, which was i) already present in the sample calcined at 600 °C, and ii) formed during the combustion process at lower temperatures by the uptake of CO_2 by CaO present in the catalysts. Furthermore, the improvement in the textural properties also has a beneficial influence on the selectivity towards CO_2, drastically reducing the CO formation up to 4-fold with respect to the uncatalyzed run (Table 3).

Table 3. Soot combustion activity and selectivity results under tight contact for different C12A7 catalysts

	T_{onset} (°C)	T_p (°C)	S_{CO_2} (%)	S_{CO} (%)
Non-catalytic run	486	655	66	34
SCS-C12A7-50	479	571	71	29
@SCS-C12A7-60	405	488	92	8
@SCS-C12A7-80	437	514	91	9

4. Conclusions

In this work, the direct formation of pure crystalline C12A7 was possible via the solution combustion technique using glycine and β-alanine as fuels, under stoichiometric conditions (Φ=1). Furthermore, we successfully developed a new, efficient and potentially scalable method to produce highly pure crystalline porous mayenite with high specific surface at mild conditions by

the addition of oxalic acid as a pore generator. Moreover, the textural properties can be tuned by varying the calcination temperature making possible the formation of porous mayenite from temperatures as low as 275 °C, reaching a remarkable specific surface area of 74 $m^2 g^{-1}$ at 400 °C and displaying a large pore volume of 0.3 $cm^3 g^{-1}$, which had never been reported before. Mayenite shows to be active in the soot combustion and be a promising catalyst in oxidation catalysis. An enhancement in mayenite textural properties led to an improvement of its catalytic activity and selectivity, shifting the complete soot oxidation to lower temperatures and favoring the formation of CO_2 over CO.

Conflicts of interest

The authors declare no competing financial interest.

Acknowledgment

The authors particularly thank Prof. Yaroslav Filinchuk for his valuable help and technical support during the Rietveld refinements. We also thank the "Université catholique de Louvain" for the scholarship awarded to I. Meza-Trujillo in the frame of the "Coopération au développement" doctoral program. F.R.S.–F.N.R.S. is also thanked for the acquisition of the XRD equipment used here (project EQP UN00616F, supervisor E. M. Gaigneaux).

Appendix A. Supporting Information. Figure A.1 shows the SEM images of SCS-C12A7-50. Table A.1 gathers the SCS parameters, crystallite size, lattice parameter and phase quantification of the C12A7 powders produced with different Φ ratios. Figure A.2 depicts the Rietveld refinements patterns of @SCS-C12A7-80. Table A.2 summarizes the weight fractions for @SCS-C12A7-80 obtained from the Rietveld analysis.

Author information

Corresponding Author

*E-mail: eric.gaigneaux@uclouvain.be

References

[1] G.A. Rankin, F.E. Wright, The Ternary System CaO-Al_2O_3-SiO_2, Am. J. Sci. 39 (1915) 1–79. doi:10.2475/06.2013.01.

[2] R.W. Nurse, Phase Equilibria and Constitution of Portland Cement, in: Chem. Cem. Proc. Fourth Int. Symp., National Bureau of Standards, Washington, 1960: pp. 9–37.

[3] B. Hallstedt, Assessment of the CaO-Al_2O_3 System, J. Am. Ceram. Soc. 73 (1990) 15–23. doi:10.1111/j.1151-2916.1990.tb05083.x.

[4] P. Hewlett, Lea's Chemistry of Cement and Concrete, 2004. doi:10.1016/B978-0-7506-6256-7.50031-X.

[5] G. Hentschel, Mayenit, 12CaO·7Al_2O_3, und Brownmillerit, 2CaO·(Al,Fe)$_2O_3$, zwei neue Minerale in den Kalksteineinschlüssen der Lava des Ettringer Bellerberges, Neues Jahrb. Mineral. (1964) 22–29.

[6] H. Bartl, T. Scheller, Zur Struktur des 12CaO·7Al_2O_3, Neues Jahrb. Fur Mineral. (1970) 547–552.

[7] H. Boysen, M. Lerch, A. Stys, A. Senyshyn, Structure and oxygen mobility in mayenite ($Ca_{12}Al_{14}O_{33}$): a high-temperature neutron powder diffraction study, Acta Crystallogr. Sect. B Struct. Sci. 63 (2007) 675–682. doi:10.1107/S0108768107030005.

[8] J. Jeevaratnam, F.P. Glasser, L.S. Dent Glasser, Anion Substitution and Structure of 12CaO·7Al_2O_3, J. Am. Ceram. Soc. 47 (1964) 105–106. doi:10.1111/j.1151-

2916.1964.tb15669.x.

[9] M. Lacerda, J.T.S. Irvine, F.P. Glasser, A.R. West, High oxide ion conductivity in $Ca_{12}Al_{14}O_{33}$, Nature. 332 (1988) 525–526. doi:10.1038/332525a0.

[10] H. Hosono, Y. Abe, Occurrence of superoxide radical ion in crystalline calcium aluminate $12CaO \cdot 7Al_2O_3$ prepared via solid-state reactions, Inorg. Chem. 26 (1987) 1192–1195. doi:10.1021/ic00255a003.

[11] K. Hayashi, M. Hirano, S. Matsuishi, H. Hosono, Microporous crystal $12CaO \cdot 7Al_2O_3$ encaging abundant O^- radicals, J. Am. Chem. Soc. 124 (2002) 738–739. doi:10.1021/ja016112n.

[12] K. Hayashi, S. Matsuishi, N. Ueda, M. Hirano, H. Hosono, Maximum Incorporation of Oxygen Radicals, O_2^- and O_2^{2-}, into $12CaO \cdot 7Al_2O_3$ with a Nanoporous Structure, Chem. Mater. 15 (2003) 1851–1854. doi:10.1021/cm020959g.

[13] S. Yang, J.N. Kondo, K. Hayashi, M. Hirano, K. Domen, H. Hosono, Formation and Desorption of Oxygen Species in Nanoporous Crystal $12CaO \cdot 7Al_2O_3$, Chem. Mater. 16 (2004) 104–110. doi:10.1016/j.ssi.2004.07.057.

[14] L. Gong, Z. Lin, S. Ning, J. Sun, J. Shen, Y. Torimoto, Q. Li, Synthesis and characteristics of the C12A7-O^- nanoparticles by citric acid sol-gel combustion method, Mater. Lett. 64 (2010) 1322–1324. doi:10.1016/j.matlet.2010.03.023.

[15] K. Hayashi, N. Ueda, M. Hirano, H. Hosono, Effect of stability and diffusivity of extra-framework oxygen species on the formation of oxygen radicals in 12CaO-7Al2O3, Solid State Ionics. 173 (2004) 89–94. doi:10.1016/j.ssi.2004.07.057.

[16] K. Hayashi, M. Hirano, H. Hosono, Excess Oxygen in $12CaO \cdot 7Al_2O_3$ Studied by Thermogravimetric Analysis, Chem. Lett. 34 (2005) 586–587. doi:10.1246/cl.2005.586.

[17] Y. Dong, H. Hosono, K. Hayashi, Formation and quantification of peroxide anions in nanocages of 12CaO□7Al_2O_3, RSC Adv. 3 (2013) 18311. doi:10.1039/c3ra42521e.

[18] J. Li, F. Huang, L. Wang, S.Q. Yu, Y. Torimoto, M. Sadakata, Q.X. Li, High Density Hydroxyl Anions in a Microporous Crystal:$[Ca_{24}Al_{28}O_{64}]^{4+}\cdot 4(OH^-)$, Chem. Mater. 17 (2005) 2771–2774. doi:10.1021/cm0500354.

[19] S. Matsuishi, K. Hayashi, M. Hirano, H. Hosono, Hydride ion as photoelectron donor in microporous crystal, J. Am. Chem. Soc. 127 (2005) 12454–12455. doi:10.1021/ja053568m.

[20] J.-P. Eufinger, A. Schmidt, M. Lerch, J. Janek, Novel anion conductors – conductivity, thermodynamic stability and hydration of anion- substituted mayenite-type cage compounds C12A7:X (X = O, OH, Cl, F, CN, S, N), Phys. Chem. Chem. Phys. 17 (2015) 6844–6857. doi:10.1039/C4CP05442C.

[21] S. Matsuishi, Y. Toda, M. Miyakawa, K. Hayashi, M. Hirano, I. Tanaka, H. Hosono, High-Density Electron Anions in a Nanoporous Single Crystal: $[Ca_{24}Al_{28}O_{64}]^{4+}(4e^-)$, Science (80-.). 301 (2003) 626–629.

[22] J.T.S. Irvine, M. Lacerda, A.R. West, Oxide ion conductivity in $Ca_{12}Al_{14}O_{33}$, Mater. Res. Bull. 23 (1988) 1033–1038. doi:10.1016/0025-5408(88)90059-1.

[23] S. Fujita, K. Suzuki, M. Ohkawa, T. Mori, Y. Iida, Y. Miwa, H. Masuda, S. Shimada, Oxidative Destruction of Hydrocarbons on a New Zeolite-like Crystal of $Ca_{12}Al_{10}Si_4O_{35}$ Including O_2^- and O_2^{2-} Radicals, Chem. Mater. 15 (2003) 255–263. doi:10.1021/cm0204122.

[24] S. Yang, J.N. Kondo, K. Hayashi, M. Hirano, K. Domen, H. Hosono, Partial oxidation of methane to syngas over promoted C12A7, Appl. Catal. A Gen. 277 (2004) 239–246. doi:10.1016/j.apcata.2004.09.030.

[25] K. Sato, M. Yamaguchi, S. Fujita, K. Suzuki, T. Mori, Enhancement of the activity of calcium aluminosilicate ($Ca_{12}Al_{10}Si_4O_{35}$) for the combustion of diesel soot via the substitution of Ca^{2+} ions with transition metal ions, Catal. Commun. 7 (2006) 132–135. doi:10.1016/j.catcom.2005.09.005.

[26] S. Fujita, K. Suzuki, T. Mori, H. Masuda, Preparation of aluminum silicate, $Ca_{12}Al_{10}Si_4O_{35}$, using waste materials and its activity for combustion of hydrocarbons, J. Eur. Ceram. Soc. 25 (2005) 3479–3484. doi:10.1016/j.jeurceramsoc.2004.09.031.

[27] R. Cucciniello, A. Intiso, S. Castiglione, A. Genga, A. Proto, F. Rossi, Total oxidation of trichloroethylene over mayenite ($Ca_{12}Al_{14}O_{33}$) catalyst, Appl. Catal. B Environ. 204 (2017) 167–172. doi:10.1016/j.apcatb.2016.11.035.

[28] S. Fujita, H. Nakano, K. Suzuki, T. Mori, H. Masuda, Oxidative destruction of hydrocarbons on $Ca_{12}Al_{14-x}Si_xO_{33+0.5x}$ ($0 \leq x \leq 4$) with radical oxygen occluded in nanopores, Catal. Letters. 106 (2006) 139–143. doi:10.1007/s10562-005-9621-5.

[29] A.A. Lemonidou, I.A. Vasalos, Preparation and evaluation of catalysts for the production of ethylene via steam cracking. Effect of Operating Conditions on the Performance of $12CaO\text{-}7Al_2O_3$ Catalyst, Appl. Catal. 54 (1989) 119–138. doi:10.1016/S0166-9834(00)82360-X.

[30] M. Ruszak, S. Witkowski, P. Pietrzyk, A. Kotarba, Z. Sojka, The Role of Intermediate Calcium Aluminate Phases in Solid State Synthesis of Mayenite ($Ca_{12}Al_{14}O_{33}$), Funct. Mater. Lett. 04 (2011) 183–186. doi:10.1142/S1793604711001907.

[31] M. Ruszak, M. Inger, S. Witkowski, M. Wilk, A. Kotarba, Z. Sojka, Selective N_2O removal from the process gas of nitric acid plants over ceramic $12CaO \square 7Al_2O_3$ catalyst, Catal.

Letters. 126 (2008) 72–77. doi:10.1007/s10562-008-9619-x.

[32] D. Jiang, Z. Zhao, S. Mu, V. Phaneuf, J. Tong, Simple and Efficient Fabrication of Mayenite Electrides from a Solution-Derived Precursor, Inorg. Chem. 56 (2017) 11702–11709. doi:10.1021/acs.inorgchem.7b01655.

[33] S.N. Ude, C.J. Rawn, R.A. Peascoe, M.J. Kirkham, G.L. Jones, E. Andrew Payzant, High temperature X-ray studies of mayenite synthesized using the citrate sol-gel method, Ceram. Int. 40 (2014) 1117–1123. doi:10.1016/j.ceramint.2013.06.112.

[34] M.M. Rashad, A.G. Mostafa, D.A. Rayan, Structural and optical properties of nanocrystalline mayenite $Ca_{1\ 2}\ Al_{1\ 4}\ O_{3\ 3}$ powders synthesized using a novel route, J. Mater. Sci. Mater. Electron. 27 (2015) 2614–2623. doi:10.1007/s10854-015-4067-z.

[35] K. Ozawa, N. Sakamoto, N. Wakiya, H. Suzuki, Fabrication of $12CaO \square 7Al_2\ O_3$ powders with high specific surface area by sol – gel and ball-milling method, J. Ceram. Soc. Japan. 119 (2011) 480–463. doi:10.1016/j.jpowsour.2014.12.129.

[36] C. Li, D. Hirabayashi, K. Suzuki, Synthesis of higher surface area mayenite by hydrothermal method, Mater. Res. Bull. 46 (2011) 1307–1310. doi:10.1016/j.materresbull.2011.03.023.

[37] B. Farin, A.H.A. Monteverde V., S. Specchia, E.M. Gaigneaux, Bismuth molybdates prepared by solution combustion synthesis for the partial oxidation of propene, Catal. Today. 257 (2015) 11–17. doi:10.1016/j.cattod.2015.03.045.

[38] A. Varma, A.S. Mukasyan, A.S. Rogachev, K. V. Manukyan, Solution Combustion Synthesis of Nanoscale Materials, Chem. Rev. 116 (2016) 14493–14586. doi:10.1021/acs.chemrev.6b00279.

[39] B. Matović, M. Prekajski, J. Pantić, T. Bräuniger, M. Rosić, D. Zagorac, D. Milivojević,

Synthesis and densification of single-phase mayenite (C12A7), J. Eur. Ceram. Soc. 36 (2016) 4237–4241. doi:10.1016/j.jeurceramsoc.2016.06.014.

[40] D. a. Fumo, M.R. Morelli, A.M. Segadães, Combustion synthesis of calcium aluminates, Mater. Res. Bull. 31 (1996) 1243–1255. doi:10.1016/0025-5408(96)00112-2.

[41] A.C. Tas, Chemical Preparation of the Binary Compounds in the Calcia–Alumina System by Self-Propagating Combustion Synthesis, J. Am. Ceram. Soc. 81 (1998) 2853–2863. doi:10.1111/j.1151-2916.1998.tb02706.x.

[42] A.S. Mukasyan, P. Dinka, Novel approaches to solution-combustion synthesis of nanomaterials, Int. J. Self-Propagating High-Temperature Synth. 16 (2007) 23–35. doi:10.3103/S1061386207010049.

[43] B. Raab, H. Poellmann, Heat flow calorimetry and SEM investigations to characterize the hydration at different temperatures of different $12CaO \cdot 7Al_2O_3$ (C12A7) samples synthesized by solid state reaction, polymer precursor process and glycine nitrate process, Thermochim. Acta. 513 (2011) 106–111. doi:10.1016/j.tca.2010.11.019.

[44] J.O. Müller, D.S. Su, R.E. Jentoft, U. Wild, R. Schlögl, Diesel engine exhaust emission: Oxidative behavior and microstructure of black smoke soot particulate, Environ. Sci. Technol. 40 (2006) 1231–1236. doi:10.1021/es0512069.

[45] D. Fino, S. Bensaid, M. Piumetti, N. Russo, A review on the catalytic combustion of soot in Diesel particulate filters for automotive applications: From powder catalysts to structured reactors, Appl. Catal. A Gen. 509 (2016) 75–96. doi:10.1016/j.apcata.2015.10.016.

[46] A. Bueno-López, Diesel soot combustion ceria catalysts, Appl. Catal. B Environ. 146 (2014) 1–11. doi:10.1016/j.apcatb.2013.02.033.

[47] J. Xiong, X. Mei, J. Liu, Y. Wei, Z. Zhao, Z. Xie, J. Li, Efficiently multifunctional catalysts

of 3D ordered meso-macroporous Ce 0.3 Zr 0.7 O 2 -supported PdAu@CeO 2 core-shell nanoparticles for soot oxidation: Synergetic effect of Pd-Au-CeO 2 ternary components, Appl. Catal. B Environ. 251 (2019) 247–260. doi:10.1016/j.apcatb.2019.03.078.

[48] Q. Wu, J. Xiong, Y. Zhang, X. Mei, Y. Wei, Z. Zhao, J. Liu, J. Li, Interaction-Induced Self-Assembly of Au@La 2 O 3 Core-Shell Nanoparticles on La 2 O 2 CO 3 Nanorods with Enhanced Catalytic Activity and Stability for Soot Oxidation, ACS Catal. 9 (2019) 3700–3715. doi:10.1021/acscatal.9b00107.

[49] Q. Wu, M. Jing, Y. Wei, Z. Zhao, X. Zhang, J. Xiong, J. Liu, W. Song, J. Li, High-efficient catalysts of core-shell structured Pt@transition metal oxides (TMOs) supported on 3DOM-Al 2 O 3 for soot oxidation: The effect of strong Pt-TMO interaction, Appl. Catal. B Environ. 244 (2019) 628–640. doi:10.1016/j.apcatb.2018.11.094.

[50] J. Xiong, Q. Wu, X. Mei, J. Liu, Y. Wei, Z. Zhao, D. Wu, J. Li, Fabrication of Spinel-Type Pd x Co 3- x O 4 Binary Active Sites on 3D Ordered Meso-macroporous Ce-Zr-O 2 with Enhanced Activity for Catalytic Soot Oxidation, ACS Catal. 8 (2018) 7915–7930. doi:10.1021/acscatal.8b01924.

[51] R. Ianoş, I. Lazău, C. Păcurariu, P. Barvinschi, Fuel mixture approach for solution combustion synthesis of Ca_3 Al_2 O_6 powders, Cem. Concr. Res. 39 (2009) 566–572. doi:10.1016/j.cemconres.2009.03.014.

[52] S.R. Jain, Energetics of Propellants, Fuels and Explosives; a chemical valence approach, Propellants Explos. 12 (1987) 188–195. doi:10.1002/prep.19870120603.

[53] A. Civera, M. Pavese, G. Saracco, V. Specchia, Combustion synthesis of perovskite-type catalysts for natural gas combustion, Catal. Today. 83 (2003) 199–211. doi:10.1016/S0920-5861(03)00220-7.

[54] S.L. González-Cortés, F.E. Imbert, Fundamentals, properties and applications of solid catalysts prepared by solution combustion synthesis (SCS), Appl. Catal. A Gen. 452 (2013) 117–131. doi:10.1016/j.apcata.2012.11.024.

[55] S. Graulis, D. Chateigner, R.T. Downs, A.F.T. Yokochi, M. Quirós, L. Lutterotti, E. Manakova, J. Butkus, P. Moeck, A. Le Bail, Crystallography Open Database - An open-access collection of crystal structures, J. Appl. Crystallogr. 42 (2009) 726–729. doi:10.1107/S0021889809016690.

[56] J. Rodríguez-Carvajal, Recent advances in magnetic structure determination by neutron powder diffraction, Phys. B Condens. Matter. 192 (1993) 55–69. doi:https://doi.org/10.1016/0921-4526(93)90108-I.

[57] J. Roisnel, J. Rodriguez-Carvajal, WinPLOTR: a Windows tool for powder diffraction patterns analysis Materials Science Forum, in: R. Delhez, E.J. Mittenmeijer (Eds.), Proc. Seventh Eur. Powder Diffr. Conf. (EPDIC 7), 2000: pp. 118–123.

[58] P. Palmisano, N. Russo, P. Fino, D. Fino, C. Badini, High catalytic activity of SCS-synthesized ceria towards diesel soot combustion, Appl. Catal. B Environ. 69 (2006) 85–92. doi:10.1016/j.apcatb.2006.06.002.

[59] S. Biamino, C. Badini, Combustion synthesis of lanthanum chromite starting from water solutions: Investigation of process mechanism by DTA-TGA-MS, J. Eur. Ceram. Soc. 24 (2004) 3021–3034. doi:10.1016/j.jeurceramsoc.2003.10.005.

[60] B. Pacewska, M. Keshr, Thermal transformations of aluminium nitrate hydrate, Thermochim. Acta. 385 (2002) 73–80. doi:10.1016/S0040-6031(01)00703-1.

[61] S. Specchia, C. Galletti, V. Specchia, Solution Combustion Synthesis as intriguing technique to quickly produce performing catalysts for specific applications, in: Stud. Surf.

Sci. Catal., 2010: pp. 59–67. doi:10.1016/S0167-2991(10)75008-4.

[62] R. Ianoş, M. Bosca, R. Lazău, Fine tuning of $CoFe_2O_4$ properties prepared by solution combustion synthesis, Ceram. Int. 40 (2014) 10223–10229. doi:10.1016/j.ceramint.2014.02.110.

[63] R. Fischer, H.J. Kuzel, Reinvestigation of the system $C_4A\square nH2O$-$C_4A\square CO_2\ \square nH_2O$, Cem. Concr. Res. 12 (1982) 517–526. doi:10.1016/0008-8846(82)90066-7.

[64] M. François, G. Renaudin, O. Evrard, A cementitious compound with composition $3CaO\square Al_2O_3\ \square CaCO_3\ \square 11H_2O$, Acta Crystallogr. Sect. C Cryst. Struct. Commun. 54 (1998) 1214–1217. doi:10.1107/S0108270198004223.